This paper is published in Proceedings of International Symposia on Materials Science for the 21th Century (ISMS-21), vol. A (The Society of Materials Science, Japan, Suita, Japan, 2001), p. 220-233.

Commentary on Atomistic Simulations of Materials Strength and Deformation: Prospects for Mechanistic Insights

Ju Li, Wei Cai, Jinpeng Chang and Sidney Yip

Department of Nuclear Engineering, Massachusetts Institute of Technology, Cambridge, MA 02139, USA

Abstract: Multiscale materials modeling has emerged as a significant concept in computational materials research. We examine several case studies which seek to provide understanding of mechanical behavior of solids at the atomistic level, in the context of upper and lower limits to strength and deformation, the interplay between melting and stability criteria, the competition between pressure-induced polymorphism and amorphization, the role of kink mechanism in dislocation mobility, and the concept of a local free energy as an invariant measure of defect driving force. Through these illustrations we express the optimistic belief that further pursuits of this kind would be worthwhile.

Key words: *melting, stability criteria, dislocation mobility, local free energy*

1. Introduction

Understanding materials behavior at the atomic level has long been a grand challenge to scientists and engineers across many disciplines. Currently the interest in identifying problems in computational materials research that offer the prospects of fundamental advances along with technological innovations has become intensified and widespread [1]. To provide a basis for such inquiries, a particular focus on atomistic simulations has emerged in the context of multiscale approach to materials theory and simulation [2, 3]. Our aim here, on the occasion of the 50th anniversary celebration of the Society of Materials Science, Japan, is to examine, through selected investigations of phase stability and defect mobility, how atomistic simulations can lead to insights into the basic mechanisms underlying the strength and deformation of solids.

We will begin in Sec. 2 by considering measures of strength through elastic and vibrational stability criteria which set the upper limit on theoretical strength. Expanding on this theme we then consider studies of melting in Sec. 3 and pressure-induced structural transitions in Sec. 4 to bring out the distinction between thermodynamic and mechanical melting and the role of chemical disorder in solid-state amorphization. In the process we find that Born's criteria on melting and stability can be unified, and the competition between polymorphism and crystal-to-amorphous transitions clarified. Lower limits of strength in real materials are often governed by the mobility of the defect microstructure. We discuss in Sec. 5 a kinetic Monte Carlo study of kink mechanism in dissociated screw dislocations in Si to illustrate how one can overcome the problem of bridging the space and time scales between atomistics and experiments.

Atomistic simulations of defect microstructure evolution are clearly central to the understanding of strength and deformation in terms of stress-strain responses. However, the concept of stress field may be inapplicable at the nanometer level, while the concept of energy remains well-defined in the manner of an interatomic potential. In Sec. 6 we suggest a local formulation of the thermodynamic driving force to move a defect. By decomposing the system into a core zone connected to the remainder through a buffer layer and deriving a tractable method of local free-energy calculation, we find results for the free energy change in a defect displacement confirming its invariance to the size of the core region. It is also noteworthy that defect-environment interactions can be highly local. To conclude our commentary brief remarks on multiscale materials modeling are offered in Sec. 7.

2. Theoretical Limits to Strength

Material strength can be defined in terms of mechanical stability. For a crystal lattice stability conditions can be formulated which specify the critical level of external stress that the system can withstand. Lattice stability is not only one of the most central issues in elasticity, it is also fundamental in any analysis of structural transformations in solids, such as polymorphism, amorphization, fracture or melting. It was first shown by M. Born that by expanding the internal energy of a crystal in a power series in the strain and requiring positivity of the energy, one obtains a set of

conditions on the elastic constants of the crystal that must be satisfied to maintain structural stability [4,5]. This leads to the determination of ideal strength of perfect crystals as an instability phenomenon, a concept that has been examined by Hill [6] and Hill and Milstein [7], as well as used in various applications [8].

That Born's results are valid only when the lattice is not under external stress was brought out explicitly in a derivation by Wang *et al* [9] invoking the formulation of a path-dependent Gibbs integral. The limitation is most displayed by considering the relation between two second-rank tensors, the elastic stiffness coefficients B and the elastic constants C [10],

$$B_{ijkl} = C_{ijkl} + \Lambda_{ijkl}, \tag{1}$$

where

$$\Lambda_{ijkl} = \frac{1}{2}(\delta_{ik}\tau_{jl}+\delta_{jk}\tau_{il}+\delta_{il}\tau_{jk}+\delta_{jl}\tau_{ik}-2\delta_{kl}\tau_{ij}), \tag{2}$$

with δ_{ij} being the Kronecker delta symbol and τ_{ij} being the applied stress tensor. The condition for the onset of elastic instability is [9],

$$\det|\mathbf{A}| = 0, \tag{3}$$

where,

$$A_{ijkl} = \frac{1}{2}\left(B_{ijkl} + B_{klij}\right). \tag{4}$$

In the absence of an external stress the elastic stiffness coefficients are the same as the elastic constants, in which case Eq.(3) gives the Born criteria. Conversely, at finite external stress lattice stability, or strength, is in principle not an intrinsic material property as are the elastic constants. In the derivation of Eq.(3) [9] the origin of the term Λ_{ijkl} arises clearly from the work done by the external stress. Further discussions of Eq.(3) has been given by Zhou and Joos [11] regarding thermodynamic (ensemble) implications and the deformation path, and by Morris and Krenn [12] regarding compatibility with the condition for internal stability formulated by Gibbs in 1876.

The connection between stability criteria and theoretical strength is rather straightforward. For a given applied stress one can imagine evaluating the current elastic constants to obtain the stiffness coefficients $\mathbf{B}$. Then by increasing the magnitude of stress one will reach a point where one of the eigenvalues of the symmetric matrix $\mathbf{A}$ (cf. Eq.(3)) vanishes. This critical stress at which the system becomes structurally unstable is then a measure of the theoretical strength of the solid. In view of this, one has a direct approach to strength determination through atomistic simulation of the structural instability under a prescribed loading. If the simulation is performed by molecular dynamics, temperature effects can be taken into account naturally by following the particle trajectories at the temperature of interest.

Under a uniform load the deformation of a single crystal is homogeneous up to the point of structural instability. For a cubic lattice under an applied hydrostatic stress, the load-dependent stability conditions are particularly simple, being of the form,

$$C_{11} + 2C_{12} + P > 0, C_{11} - C_{12} - 2P > 0, C_{44} - P > 0, \tag{5}$$

where P is positive (negative) for compression (tension), and the elastic constants C_{ij} are to be evaluated at the current state. While this result is known for some time [13–15], direct verification against atomistic simulations showing that the criteria do accurately describe the critical value of P (P_c) at which the homogeneous lattice becomes unstable has been relatively recent [9, 16–20]. One may therefore regard P_c as a definition of the theoretical or ideal compressive (tensile) strength of the elastic body.

One may regard the stability criteria, Eq.(5), as manifestation in the long wavelength limit of the general condition for vibrational stability of a lattice. The vanishing of elastic constants then corresponds to the phenomenon of soft phonon modes in lattice dynamics. Indeed one finds that under sufficient deformation such soft modes do occur in a homogeneously strained lattice. To see the lattice dynamical manifestation of this condition, we apply molecular dynamics to relax a single crystal sample with periodic boundary condition at essentially zero temperature for a specified deformation at constant strain. The resulting atomic configurations are then used to construct the dynamical matrices which are then diagonalized. Fig. 1 shows two sets of dispersion curves for fcc Ar at 0K described by the Lennard-Jones interatomic potential ($r_c = 2.5\sigma$), one for the crystal at equilibrium (for reference) and the other when the lattice is deformed under a uniaxial tensile strain of 0.138 which is close to the critical value [21]. One can see in the latter a Γ-point soft mode in the [011] direction. Similar results for deformation under shear or hydrostatic tensile strain would show Γ-point soft modes in the [111] and [100] directions, respectively. All these are acoustic zone-center modes, therefore they would correspond to elastic instabilities. For a more complicated lattice such as SiC in the zinc blende structure, one would find that soft modes also can occur at the zone boundaries [21]. The overall implication here is that lattice vibrational analysis of a deformed crystal offers the most general measure of structural instability at 0K, and this again demonstrates that strength is not an intrinsic property of the material, rather it depends on the mode of deformation.

Returning to molecular dynamics simulations we

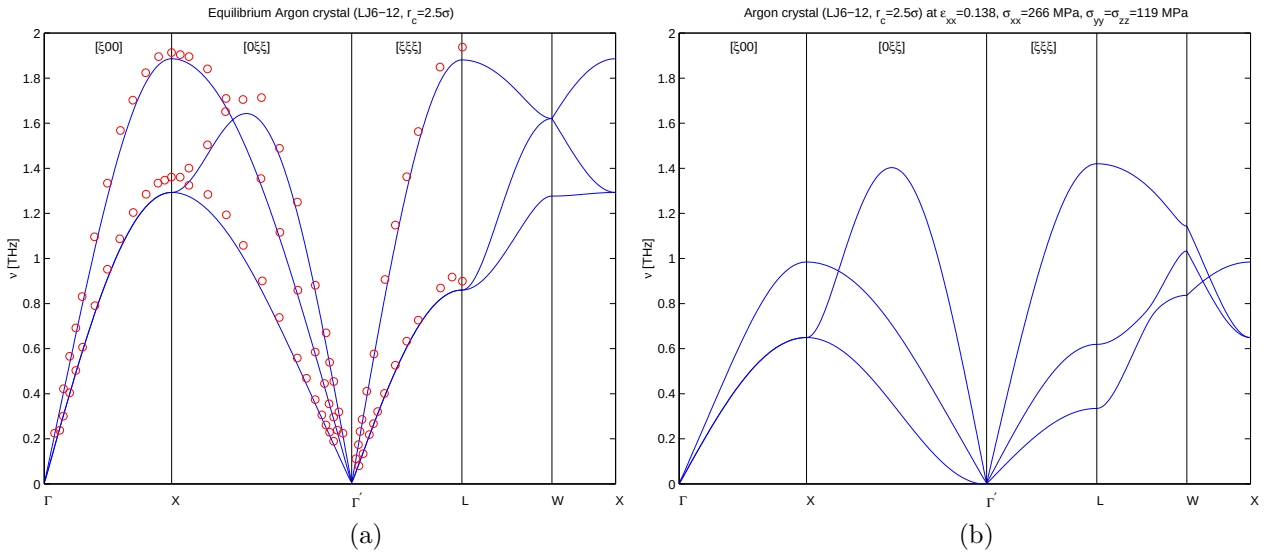

Figure 1: Phonon dispersion curves of single crystal of Ar as described by the Lennard-Jones potential (solid lines), (a) comparison of results for equilibrium condition with experimental data (^{36}Ar results (circles) are rescaled for $m = 39.948$ amu) [59], (b) results for uniaxial tension deformation at strain of 0.138, corresponding stresses of 266 MPa and 119 MPa along the tensile and transverse direction. The labeling tracks only one split branch of the original cubic-symmetry **k**-point. [21]

show in Fig. 2 the stress-strain response for a single crystal of Ar under uniaxial tension at 35.9K. At every stage of fixed strain, the system is relaxed and the stress tensor evaluated. One sees the expected linear elastic response at small strains up to about 0.05; thereafter the response is nonlinear but still elastic up to a critical strain of 0.1 and corresponding stress of 130 MPa. Applying a small increment strain beyond this point causes a dramatic stress reduction (relief) at point (b). Inspection of the atomic configurations at the indicated points shows the following. At point (a) several point defect like inhomogeneities have been formed; most probably one or more will act as nucleation sites for a larger defect which causes the strain energy to be abruptly released. At the cusp, point (b), one can clearly discern an elementary slip on an entire [111] plane, the process being so sudden that it is difficult to capture the intermediate configurations. Figuratively speaking, we suspect that a partial dislocation loop is spontaneously created on the (111) plane which expands at a high speed to join with the dispersed inhomogeneities until it annihilates with itself on the opposite side of the periodic border of the simulation cell, leaving a stacking fault plane. As one increases the strain the lattice loads up again until another slip occurs. At (c) one finds that a different slip system is activated.

What we have seen here in Fig. 2 is a typical stress-strain response on which one can conduct very detailed analysis of the deformation using the atomic configuration available from the simulation. This atomic-level version of structure-property correlation can be even more insightful than the conventional macroscopic counterpart simply because in simulation the microstructure can be as well characterized as one desires. As an illustration we consider the single-crystal response such as that shown in Fig. 2 a reference and repeat the deformation simulation using initial atomic configurations which have some distinctive microstructural features. We have performed such studies on SiC using prepared amorphous and nanocrystalline structures [21]. In this case the single-crystal reference at $T = 1300$K, under pure shear rather than uniaxial tension, shows a similar linear elastic response at small strain up to about 0.05; thereafter the response is nonlinear but still elastic up to a critical strain of $\epsilon_{xy} = 0.18$ and corresponding stress of $\sigma_{xy} = 43$ GPa. Applying a small increment strain beyond this point causes a dramatic change, similar to that seen at point (a) in Fig. 2, with the internal stress suddenly reduced by a factor of 3. Inspection of the atomic configurations shows the nucleation of an elliptical microcrack in the lattice along the direction of maximum tension. With further strain increments the specimen deforms by strain localization around the crack with essentially no change in the system stress.

The responses of the amorphous and nanocrystalline SiC differ significantly from that of the single crystal under hydrostatic tension. The former shows a broad peak, at about half the critical strain

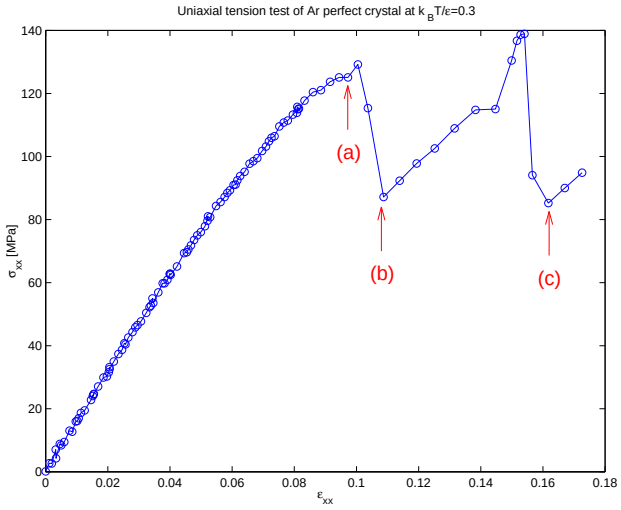

Figure 2: Atomistic stress-strain response of a single crystal of Ar under uniaxial tensile deformation at constant strain at a reduced temperature of 0.3 (35.9K), simulation data are indicated as circles and solid line is drawn to guide the eye. [21]

and stress, suggesting a much more gradual structural transition. Indeed, the deformed atomic configuration reveals channel-like decohesion at strain of 0.096 and stress 22 GPa. Another feature of the amorphous sample is that the response to other modes of deformation, uniaxial tension and shear, is much more isotropic relative to the single crystal, which is perhaps understandable with bonding in SiC being quite strongly covalent and therefore directionally dependent. For the nanocrystal, the critical strain and stress are similar to the amorphous phase, except that the instability effect is much more pronounced, qualitatively like that of the single crystal. The atomic configuration shows rather clearly the failure process to be intergranular decohesion. These observations allow us to correlate the qualitative behavior of the stress-strain responses with a gross feature of the system microstructure, namely, the local disorder (or free volume). This feature is completely absent in the single crystal, well distributed in the amorphous phase, and localized at the grain boundaries in the nanocrystal. The disorder can act as a nucleation site for structural instability, thereby causing a reduction of the critical stress and strain for failure. Once a site is activated, it will tend to link up with neighboring activated sites, thus giving rise to different behavior between the amorphous and nanocrystalline samples.

3. Unifying Born's Melting and Stability Criteria

In 1939 Born set forth a simple criterion for crystal melting by postulating that melting should be accompanied by the loss of shear rigidity [22]. Expressed in terms of the shear modulus G for a cubic crystal, the melting point T_m is the temperature at which,

$$G(T_m) = 0. \tag{6}$$

A year later he extended this stability concept to lattice deformation [4] by deriving the well-known conditions for mechanical stability, valid for cubic crystals,

$$C_{11} + 2C_{12} > 0,\ C_{11} - C_{12} > 0,\ C_{44} > 0, \tag{7}$$

where C_{11}, C_{12} and C_{44} $(= G)$ are the three distinct elastic constants (in Voigt notation).

In this section we will examine the basis on which Born's two criteria may be considered to be valid. Shortly after Eq.(6) was proposed, experimental results obtained on NaCl single crystals were presented showing that the two shear constants, C_{44} and $C_{11} - C_{12}$, have nonzero values at the melting point [23]. Moreover, it was not clear how this criterion could explain the existence of latent heat and volume change in a first-order thermodynamic phase transition. In contrast, the stability criteria Eq.(7) seem to be generally accepted, with neither stringent tests having been performed nor qualifications concerning its possible limitations discussed. The challenge of ascertaining whether such criteria are capable of predicting the actual onset of an instability is considerable. The difficulty, on the theoretical side, has been that stability analyses have been formulated in different ways [9,10], and few explicit calculations of elastic constants at the critical condition have been reported to make possible an unambiguous test. On the experimental side, competing effects frequently render the determination of the triggering instability uncertain. Thus, while the shortcomings of Eq.(7) are well known, the use of Eq.(7) to define structural resistance to thermal agitation has gone unnoticed.

Our interest is to test Eq.(7) through molecular dynamics simulation of melting instead of testing Eq.(6) using experimental data. By performing simulation of isobaric heating to melting at zero pressure of a perfect crystal without surfaces or defects of any kind, we achieve an unambiguous test since without an external stress Eq.(7) would be equivalent to Eq.(5). As we will see below, simulation shows that at the onset of melting one of the shear constants indeed vanishes, although it is $C_{11}-C_{12}$ rather than C_{44}. The observed melting temperature, or equivalently the critical lattice strain, is in remarkable agreement with the predictions based on the stability criteria. Since the system is initially a defect- and surface-free lattice, the homogeneous melting observed here is to be distinguished from the conventional melting which is a free-energy

based heterogeneous process of nucleation and growth. The latter process, if not kinetically suppressed in simulation by eliminating all defects and surfaces, would set in at a lower temperature, the conventional melting point of the material, and preclude the melting process associated with an elastic instability. Allowing for these modifications, the melting and stability criteria proposed by Born are reconciled. The qualification which is nontrivial is that the concept of thermoelastic mechanism of melting indeed applies to a form of melting, but it is melting in the sense of mechanical stability against thermal excitation as opposed to the conventional thermodynamic process which is always defect mediated and therefore heterogeneous.

Given that the generalized criteria Eq.(5) obviously reduce to Born's results in the limit of zero load, Eq.(7) is a valid description of lattice stability in the special case of a cubic crystal being heated to melting at zero pressure. For the simulation we use an interatomic potential model for Au [24] (details of the potential are of no interest in this discussion) and a simulation cell containing $1,372$ atoms with periodic border conditions imposed in the manner of Parrinello and Rahman [25]. A series of isobaric-isothermal simulations are carried out at various temperatures. At each temperature the atomic trajectories generated are used to compute the elastic constants at the current state using appropriate fluctuation formulas [26].

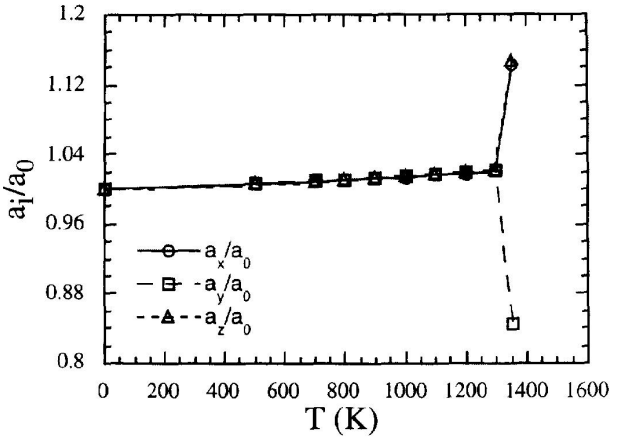

Figure 3: Variation of lattice strain a/a_0 with temperature along three Cartesian directions in the simulation of an isobaric ($P = 0$) heating process.

Fig. 3 shows the variation with temperature of the lattice strain a/a_0 along the three cubic symmetry directions [27]. The slight increase with increasing temperature merely indicates the lattice is expanding normally with temperature, and the results for the three directions are the same as they should be. At $T = 1350$K one sees a sharp bifurcation in the lattice dimension where the system elongates in two directions and contracts in the third. This is a clear sign of symmetry change, in the present case from cubic to tetragonal. To see whether the simulation results are in agreement with the prediction based on Eq.(7), we show in Fig. 4 the variation of the elastic moduli with temperature, or equivalently the lattice strain since there is a one-to-one correspondence as indicated in Fig. 3; the three moduli of interest are the bulk modulus $B_T = (C_{11} + 2C_{12})/3$, tetragonal shear modulus $G' = (C_{11} - C_{12})/2$, and rhombohedral shear modulus $G = C_{44}$. On the basis of Fig. 4 one would predict the incipient instability to be the vanishing of G', occurring at the theoretical or predicted lattice strain of $(a/a_0)_{\text{theory}} = 1.025$. From the simulation at $T = 1350$K the observed strain is $(a/a_0)_{\text{observed}} = 1.024$. Thus, we can conclude that the vanishing of tetragonal shear is responsible for the structural behavior.

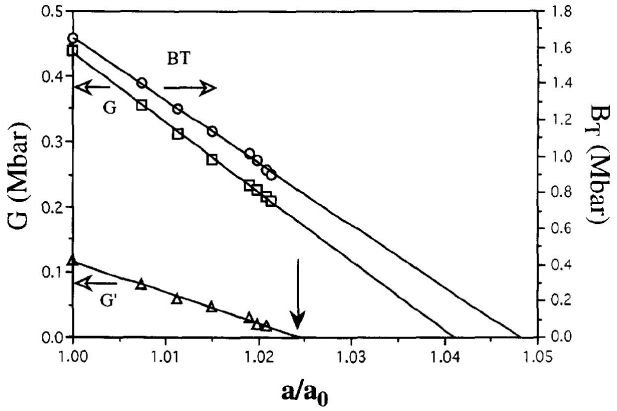

Figure 4: Variation of B_T, G, and G' with lattice strain a/a_0 in the isobaric ($P = 0$) heating process.

For more details of the system behavior at $T = 1350$K we show in Fig. 5 the time evolution of the lattice strain, the off-diagonal elements of the cell matrix $\mathbf{H}$, and the system volume. It is clear from Fig. 5(a) that the onset of the $G' = 0$ instability triggers both a shear (cf. Fig. 5(b)) and a lattice decohesion (Fig. 5(c)), the latter providing the characteristic volume expansion associated with melting. This sequence of behavior, which has not been recognized previously, implies that the signature of a first-order transition, namely, latent volume change, is not necessarily associated with the incipient instability. Our results also provide evidence supporting Born's picture of melting being driven by a thermoelastic instability [22], later reinterpreted by Boyer [28] to involve a combination of loss of shear rigidity and vanishing of the compressibility. Moreover, it is essential to recognize that this thermoelastic mechanism can only be applied to the process of mechanical instability (homogeneous melt-

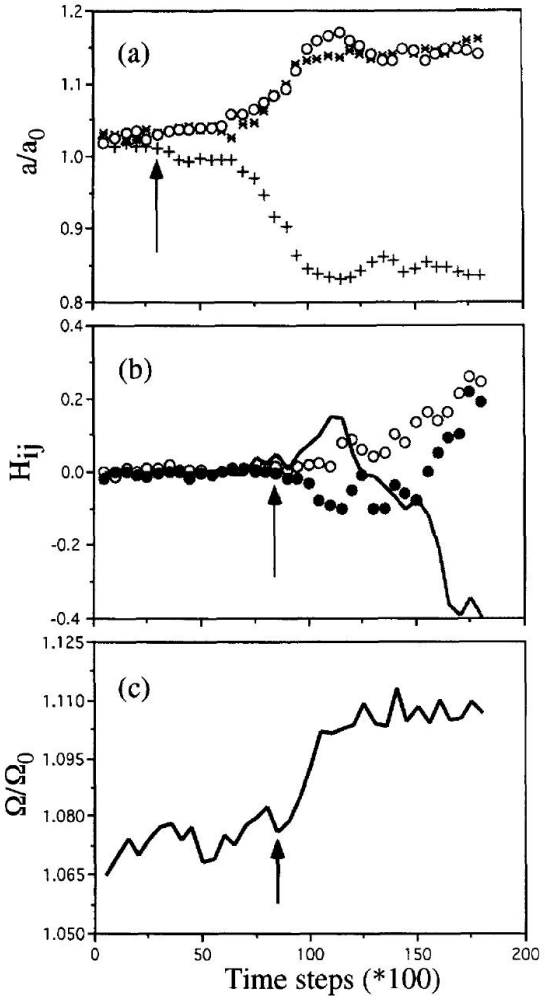

Figure 5: Time responses of (a) lattice strain along three initially cubic directions, (b) off-diagonal elements of the cell matrix **H**, H_{12}, H_{13}, H_{23}, (c) normalized system volume. Arrow indicate the onset of Born instability in (a), shear instability in (b), and lattice decohesion in (c).

ing) of a crystal lattice without defects, and not to the coexistence of solid and liquid phases at a specific temperature (heterogeneous melting) [29,30].

It is perhaps worthwhile emphasizing again what the combination of stability analysis and molecular dynamics simulation has contributed to the understanding of Born's two criteria. That the stability criteria Eq.(7) are valid only under vanishing external load is quite clear, both theoretically and in simulation studies. Since it is often advantageous to be able to predict a priori the critical stress or strain for the onset of instability, the availability of Eq.(5) could facilitate more quantitative analysis of simulation results. Although our results for an fcc lattice with metallic interactions show that homogeneous melting is triggered by $G' = 0$ and not Eq.(6), nevertheless, they constitute clear-cut evidence that a shear instability is responsible for initiating the transition. The fact that simulation reveals a sequence of responses apparently linked to the competing modes of instabilities (cf. Fig. 5) implies that it is no longer necessary to explain all the known characteristic features of melting on the basis of the vanishing of a single modulus. In other words, independent of whether $G' = 0$ is the initiating mechanism, the system will in any event undergo volume change and latent heat release in sufficiently rapid order (on the time scale of physical observation) that these processes are all identified as part of the melting phenomenon. Generalizing this observation further, one may entertain the notion of a hierarchy of interrelated stability catastrophes of different origins, elastic, thermodynamic, vibrational, and entropic [31].

Finally it may be mentioned that in several studies over the last few years, the stability criteria Eq.(5) have lead to precise identifications of the elastic instability triggering a particular structural transition. In hydrostatic compression of Si, the instability which causes the transition from diamond cubic to β-tin structure is the vanishing of $G'(P) = (C_{11} - C_{12} - 2P)/2$ [17]. In contrast, compression of crystalline SiC in the zinc blende structure results in an amorphization transition associated with the vanishing of $G(P) = C_{44} - P$ [20]. This is discussed further in the next section. For behavior under tension, crack nucleation in SiC [18] and cavitation in a model binary intermetallic [19], both triggered by the spinodal instability, vanishing of $B_T(P) = (C_{11} + 2C_{12} + P)/3$, are results which are analogous to the observations reported here. Notice also that in the present study a crossover from spinodal to shear instability can take place at sufficiently high temperature [9].

4. Competing Mechanisms in Pressure-Induced Structural Transitions

When a homogeneous lattice without defects of any kind is driven to structural instability by hydrostatic compression, two types of responses generally can be expected, a polymorphic transition to another lattice structure, or a transition to a disordered state, a phenomenon known as solid-state amorphization. Molecular dynamics simulations of compression loading on Si [17] and cubic SiC (β-phase) [20] using essentially the same many-body interatomic interaction model have shown that the former undergoes a transition from diamond cubic to β-tin tetragonal structure, while the latter undergoes amorphization. The behavior of stability criteria in these two studies are shown in Fig. 6, where one sees that the two transitions involve different instability modes, the vanishing of the

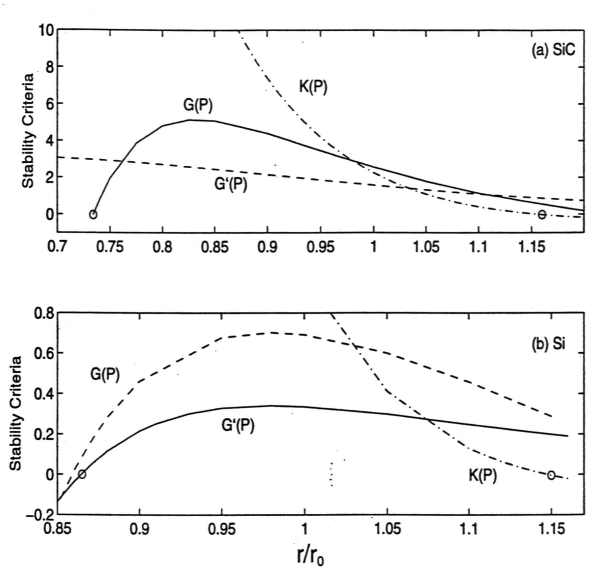

Figure 6: Variation of the elastic moduli, K, G, and G', with lattice strain under hydrostatic loading at 0K, (a) β-SiC, (b) Si. $r/r_0 = 1$ denotes the condition of zero stress.

tetragonal shear modulus G' and the rhombohedral shear modulus G, respectively. The potential models from which the elastic constants are calculated are of the same bond-order form proposed by J. Tersoff [32] for covalent crystals. In both cases, the critical strains predicted in Fig. 6 agreed with what was observed in the direct simulations. The question then arises as to what is the underlying cause of the different structural consequences of shear instability.

Table 1: Calculated properties of the Tersoff model for β-SiC and its two modifications [20].

	Tersoff	Model I	Model II
lattice constant[Å]	4.32	4.34	4.32
cohesive energy[eV]	-6.18	-6.03	-6.18
bulk modulus[GPa]	225	218	225
C_{11}[GPa]	436	419	331
C_{12}[GPa]	120	117	172
C_{44}[GPa]	255	242	161
$C_{11} - C_{12}$[GPa]	316	302	159

It is apparent that an obvious difference between the two lattices is that one is an elemental system while the other is a binary (AB) compound. Thus in SiC there are chemical ordering effects which are not present in Si. Since in the context of chemical ordering a distinction is made between atomic size effects and chemical bonding effects, it is of interest to assess which effect is more responsible for the observed amorphization. For this analysis one can manipulate the description of interatomic interactions to intentionally suppress one effect or the other. Two modified forms of the Tersoff potential model have been produced, in one variant chemical bond preference is suppressed through an adjustment of the interaction between atoms of different species (model I), and in another variant size effects are suppressed by adjusting the bond-order parameter and cross interaction at the same time to leave heat of mixing unchanged (model II) [33]. The relevant physical properties of the Tersoff potential for β-SiC and its two modifications are shown in Table I. It is clearly seen that elimination of chemical bonding preference has little effect (model I), whereas all three elastic constants are significantly altered in the absence of atomic size difference. Although both $C_{11} - C_{12}$ and C_{44} are appreciably reduced, the lowering of the former is more drastic such that in model II the instability mode becomes the vanishing of G'. Thus one may deduce that not only is the presence of size effects responsible for the rhombohedral shear instability in β-SiC, but also their absence allows the tetragonal shear to vanish first in Si. To explicitly verify that these interpretations are correct, a simulation of model II under compression was carried out, indeed revealing a transition from zinc-blende to rock salt structure triggered by a tetragonal shear instability. This is an illustration of the use of modified or manipulated interatomic interaction in simulation; it can be a potentially very useful device for isolating cause-and-effect in probing complex phenomena.

We have demonstrated that in terms of the competition between instability modes, in this case the vanishing of the two shear moduli, one can gain some insight into the underlying nature of polymorphic and crystal to amorphous transitions. With regard to the experimental implications of our results on β-SiC, we note that amorphization of β-SiC single crystals induced by electron irradiation have been reported [34], the data revealing chemical disordering to take place below a critical temperature of 340°C. On the other hand, the structural transition in β-SiC under compression is found by X-ray diffraction to be polymorphic, from zinc-blende to a rock salt-type structure at 100 GPA [35]. The reason that the simulation predictions do not match precisely with the experimental findings can be attributed to two factors. First is that the empirical classical interatomic potential description is likely not adequate to correctly resolve competing mechanisms involving subtle effects of chemical bonding. Secondly, the role of crystal defects in controlling the experimental observations has not been quantitatively assessed, while for the simulations one knows for sure that no defects were initially present. These uncertainties aside, it is noteworthy that both amorphization and polymorphic transitions have been

observed in β-SiC. Apparently, under the relatively "gentle" driving force of pressure the latter, associated with $G' = 0$, prevails over the former which entails $G = 0$. The driving force induced by electron irradiation is the destabilizing effect of point defect production; under this condition β-SiC undergoes amorphization rather than transforming to another crystal structure.

Even though in β-SiC pressure-induced amorphization appears to be precluded by a polymorphic transition, several experimental studies of this phenomenon in AB compounds can be cited to provide further insights into the kinetics of competing transitions. X-ray measurements show that Nb_2O_5 becomes amorphous at 19.2 GPa at 300 K which is novel because the oxide is simultaneously reduced in the process [36]; the competing polymorphic transition is believed to be kinetically impeded. In BAs a transformation from zinc blende to amorphous structure was observed at 125 GPa, just slightly above the calculated equilibrium transition pressure to the rock salt phase, and interpreted as signifying a kinetically frustrated process [37]. In more complicated systems, such as $CaSiO_3$ an $MgSiO_3$ perovskites, it has been conjectured that stress-induced amorphization arises from the near simultaneous accessibility of multiple modes of instability [38]. The amorphization of α-quartz under pressure is a particularly well-known case where molecular dynamics simulation gives a transition pressure in agreement with experiment [39]. The physical mechanism underlying the elastic instability was first identified as the softening of a phonon mode [40]; later a dynamic instability associated with a soft phonon mode at one wave vector was found [41]. These developments are not surprising in view of our discussions in Section 2. It is interesting that the dynamic instability in α-quartz precede the elastic instability, occurring at 21.5 GPa and 25 GPa respectively.

5. Dislocation Mobility in Silicon

How the motion of a single dislocation in silicon is affected by temperature and stress is a longstanding question in crystal plasticity [42]. Much of our present understanding is based on a semi-empirical theory of kink diffusion [43] which does not properly account for important mechanistic details of the processes governing dislocation glide. For example, the effects of interactions between partial dislocations in dislocations that have dissociated have been appreciated for some time [44], but we still do not know how to interpret their quantitative effects on the measured data. Recently, atomistic studies have revealed the existence of kink multiplicity [45–47], giving further impetus to seek extension beyond the standard treatment of dislocation glide via the double kink mechanism [43]. Finally, atomistic calculations ranging from empirical potential models [48, 49] to electronic structure methods based on tight-binding approximation [47] and first principles methods [50, 51] are starting to give kink formation and migration activation energies, including results specific to detailed kink structures. If these results are to be used in predicting dislocation mobility, a method is needed to relate the microscopic details on the angstrom length scale to existing mobility data measured on the micron scale.

From the standpoint of analyzing dislocation mobility on the experimental spatial and time scales, $1 - 100$ microns and $1 - 100$ milliseconds, a direct simulation using discrete atoms is well beyond the current computational capabilities. On the other hand, it is quite feasible to represent a dislocation by a large number of line segments, which individually can be allowed to evolve under the influence of temperature and applied stress. For the model to be capable of giving quantitative results, a mechanism for the displacement of an individual line segment has to be prescribed. In this discussion we will adopt the well-known mechanism of double kink nucleation and migration as the underlying process for dislocation mobility [43].

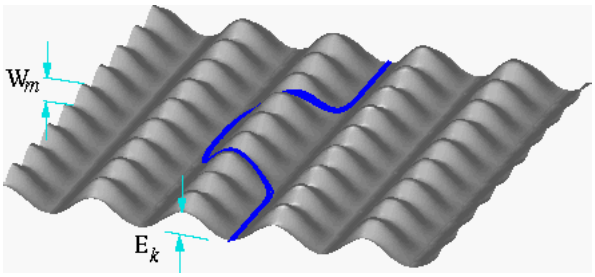

Figure 7: Kink mechanism of dislocation glide involving activation of a dislocation segment over two Peierls energy barriers, E_k and W_m, for kink nucleation and migration, respectively.

The physical picture illustrating the kink mechanism of dislocation glide is displacement of a single dislocation line on a potential energy surface with periodic barriers as shown in Fig. 7. The surface is seen to be corrugated along two directions; the heights of the barrier along the direction of displacement controlling kink nucleation and that along the transverse direction controlling kink expansion (migration) are denoted as E_k and W_m respectively. Backward activations are allowed so that a narrow double kink can annihilate, or one of the two ledges of the double kink can contract. The displacement of the entire dislocation line over arbitrary number of E_k barriers is realized by dividing the line into a large number of segments with each segment undergoing the unit glide

process depicted in Fig. 7.

The application of Monte Carlo as an energy-based method for efficiently sampling a large number of such unit events is potentially a practical solution to the time scale problem of relating mobility events occurring over periods of seconds to the underlying mechanistic processes which take place over picoseconds. At present it is still somewhat of an open question whether reasonable behavior of dislocation mobility seen by experiments can be produced by treating stochastically a large number of the unit events. The essence of the kinetic Monte Carlo, in contrast to sampling statistical ensembles for calculations of equilibrium properties, lies simply in expressing activation energy barriers for defect mobility as a rate in transition state theory which is to be sampled with every step in the simulation.

For the operation of the kink mechanism it follows there are two such rates, one for nucleation and another independent one for migration. We write the nucleation rate as,

$$j_{dk}(1) = \omega_0 \exp\left(-\frac{E_{emb} + (\pm\gamma_{\rm SF} - \vec{\tau}\cdot\vec{b}_\alpha)A/2}{k_{\rm B}T}\right), \tag{8}$$

where ω_0 is the sampling frequency factor, which we will set equal to the *Debye frequency*, $\vec{\tau} = (\sigma_{yz}, -\sigma_{xy})$ is the applied stress, $\vec{b}_\alpha = (b_z, b_x)_\alpha, \alpha = 0, 1$ are the Burgers vectors of the leading and trailing partials, $\vec{b}_0 = (b/2, b\sqrt{3}/6)$ and $\vec{b}_1 = (b/2, -b\sqrt{3}/6)$, $A = \pm bh$ is the area swept out by the dislocation during such transformation, with"+" or "−" sign for upward or downward nucleation respectively, $k_{\rm B}$ is the Boltzmann's constant and T is the temperature. The sign before $\gamma_{\rm SF}$ takes "+" or "−" for leading and trailing partials. The factor of $1/2$ appears because we assume that in the saddle point configuration the dislocation has swept out half of the total area A. A similar expression, with appropriate modifications, holds for the kink migration rate.

For the implementation of our kinetic Monte Carlo model we refer the readers to our previous reports [52, 53], here we will discuss further the physical content of the simulation and the mechanistic insights that can be extracted from the analysis. One should note that there are a total of four energies entering in our description, the activation energies for kink nucleation and migration, E_k and W_m, the stacking fault energy, $\gamma_{\rm SF}$, and the elastic interaction energy between a given segment and all the other segments and the applied stress (so-called Peach-Koehler interaction), $E_{\rm PK}$. The first two are necessary for describing the displacement of a straight dislocation line through the double-kink mechanism, the third appears because the dislocation is dissociated so the line is actually an elastic ribbon, and finally the elastic interaction is needed to account for the local dislocation microstructure as well as the external applied stress. With kink nucleation or migration coupled to expansion or contraction of the stacking-fault ribbon, and the elastic interactions, our model can be expected to be able to account for nontrivial behavior of the dislocation velocity.

Table 2: Kink's formation energy E_k and migration barrier W_m (in eV) on 30° and 90° partials in silicon obtained from atomistic calculations using EDIP potential, tight-binding (TB) and density functional theory (DFT), and experimental measurements using transmission electron microscopy (TEM) and high resolution electron microscopy (HREM).

		30°		90°	
		E_k	W_m	E_k	W_m
EDIP	[60]	0.52	0.89	0.70	0.62
TB	[47]	0.82	1.52	0.12	1.62
DFT	[61]		2.1		
DFT	[50]			0.1	1.8
DFT	[51]			0.04	1.09
TEM	[62]			≥0.4	≤1.2
TEM	[63]		1∼1.2		1∼1.2
HREM	[64]	0.8	1.55	0.74	1.55

Of the four energies in our formulation, the determination of the kink nucleation and migration activation energies poses the most direct challenge to atomistic simulation. In Table 2 we list the literature values, experimental and calculated, for E_k and W_m. Very little agreement is seen among the theoretical predictions, which range from empirical interatomic potentials to electronic structure calculations. At the same time the experimental data also are not conclusive. Given this situation, we consider all the available information in Table 2 without favoring any particular result, and in this way arrive at a set of "effective" or estimated values, $E_k = 0.7$ eV and $W_m = 1.2$ eV [53]. By adopting these estimates, along with a reasonable ω_0 and a typical value for the entropy, we find dislocation velocities given by the kinetic Monte Carlo simulation are of the same magnitude as the measurements with satisfactory agreement in the temperature variation over a considerable range. While we are cautious in giving too much significance to this agreement, we do believe that this is an encouraging and useful result providing a guide for future calculations and measurements of kink energetics.

It could be said that obtaining the correct temperature dependence of the dislocation velocity is not a stringent test of the model, since temperature appears only as a multiplicative factor in the exponent. Without changing any parameter in our description,

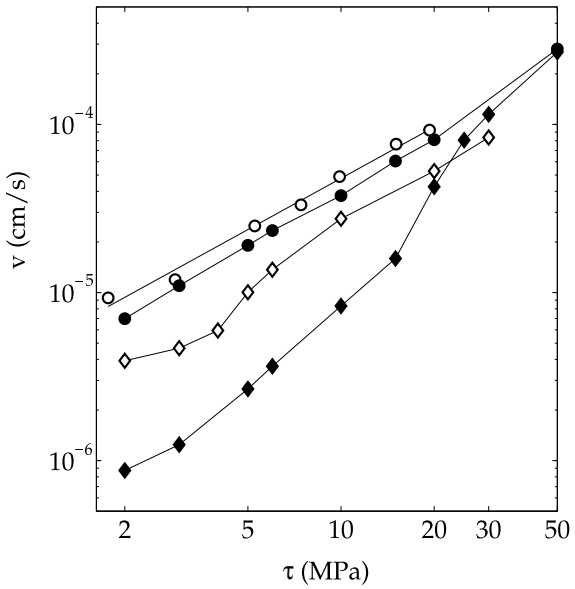

Figure 8: Stress variation of the velocity of a screw dislocation in Si at $T = 1000$ K. kMC predictions are shown in closed symbols, diamond for the commensurate condition and circle for the non-commensurate condition, while experimental data showing corresponding behavior are shown in open symbols [52]. Solid lines are drawn to guide the eye.

we now turn to examine the stress variation and find a somewhat subtle effect of the mobility of a dissociated dislocation that had not been previously appreciated. The origin of this effect lies in the coupling between the leading and trailing partials which itself involves the interplay of three factors, the Peierls barrier for a unit displacement of a partial (same as the barrier E_k for kink nucleation in Fig. 7), the cohesive action of the stacking fault ribbon between the partials, and the elastic interactions between the moving segment of partial and its local environment in the presence of an applied stress. To describe the coupling in more details, it is helpful to consider that, in the absence of the Peierls barrier, the ideal separation between the two partials would be This separation, which we denote as X_0, is given by the expression $X_0 = \mu b^2 \alpha / (\gamma_{\rm SF} - \sigma_{xy} b_x)$, where μ is the shear modulus, $\alpha = (1/4 - 1/12(1-\nu))/2\pi$, $b_x = b\sqrt{3}/6$, and ν is the Poisson ratio. The significance of X_0 is that when it is a multiple of the period of the Peierls barrier (the kink height in Fig. 7), it becomes a characteristic separation distance between the two partials with the partials strongly confined to their lowest energy configuration at the valley of the Peierls potential. We will refer to this as the commensurate condition, since at this separation for one partial to move to the next valley, the only way to avoid the inherent energy penalty is for the other partial to move in unison. Under this circumstance, the reduced mobility of the unit event may be expected to manifest in low values for the dislocation velocity at low stress on experimental scale and a sublinear variation with stress. This behavior indeed has been observed as well as measurements of a linear variation, both shown in Fig. 8.

The reasoning we have just given for the strong coupling between the partials allows, in a self-consistent manner, for a different type of mobility behavior when X_0 is not commensurate with the period of the Peierls barrier. Then the two partials can be expected to behave much more independently of each other. This can be seen by considering X_0 to be half integral multiple of the period, in which case the lowest energy state of the dissociated dislocation is doubly degenerate. Now each partial can migrate independently to the adjacent valley without penalty, provided the displacements follow appropriate sequence such that with each unit displacement the separation between the nucleated double kink and the other partial is again at the low energy state.

The simulation results in Fig. 8 demonstrate that one indeed obtains significantly different stress variations, essentially a sublinear behavior when X_0 is multiple and a linear behavior when it is half-integral multiple of the period of the Peierls barrier. Compared to the experimental data we see rather good agreement in the case of linear stress variation, and qualitatively similar behavior for the threshold effect. The latter is not unreasonable given that the measurements are necessarily averages over a range of local conditions whereas the prediction is strictly for the case of commensurate barrier. We should also add that the threshold effect should manifest only at low stresses since potential barriers become less important at higher stresses. Based on our model we can estimate the critical stress where the transition may be expected, obtaining a value of 16.8 MPa, which is what is seen in Fig. 8 and compatible with another estimate based on different considerations [54].

We close this section with a final comment. The effect of coupling between the partials has been considered in the theoretical analysis of mobility of a straight dislocation [55–57]. What we have shown here is that the distinction between integral and half-integral separation applies equally well to the dislocation mobility by kink mechanism. The precise value of X_0 is determined by a number of physical properties, the stacking fault energy, the elastic constant, or any other factor which affects the dissociation width. In reality it is likely that the value of X_0 will experience significant local variations over the length of the dislocation line due to intrinsic lattice defects, dopants, impurities, stress gradients, etc., all of which can affect the lo-

cal condition of partial-partial interaction. Our simulations indicate that in locations where X_0 is near half-integer value, kinks can form and glide independently on each partial, while in other locations where X_0 is near integral value, kink formation and migration can only occur simultaneously on both partials, in the low-stress regime. Since the rates of the strongly-coupled processes are much lower, in the overall scenario of dislocation motion, kink nucleation will occur at weak or "uncorrelated" sites, followed kink propagation and arrest at the strong or "correlated" sites. An arrested kink can still pass through the strong segment if pushed from behind by kinks piling up on the same partial. Alternatively, the kink can capture a partner kink on another partial, at which point the hard segment becomes penetrable for the coupled migration of the newly formed kink pair. In either case, such "correlated" segments act as effective obstacles to kink migration. This line of argument provides a natural explanation of the "weak obstacle" effect, a concept which had been advanced to explain the unusual dislocation behavior observed in semiconductors [58].

6. Defect Driving Force - Search for a Local Invariant

In the present examination of how atomistic structures and interactions affect strength and deformation on the microscopic level, it is clear the system response is governed by the defects or microstructure present. By studying the stability of a single crystal, a system without microstructure, one obtains the upper limit or theoretical strength of the lattice, as discussed in Secs. 2 through 4. In real solids where defects are invariably present, the stress-strain response is expected to show considerably lower strength and usually more complex deformation than simple linear or nonlinear elasticity. Dislocation mobility, discussed in Sec. 5, plays an important role in providing an estimate of a lower limit to strength. A fundamental question here is the local force acting on a defect, whether it is the dislocation core or a crack tip, that causes it to move. This conceptually simple quantity is central to any physical description of mechanical behavior, yet it is surprisingly difficult to calculate. To see the bottleneck, one should rephrase the problem by asking for the force to move an isolated defect. While a single defect in an infinite and otherwise defect-free crystal is easy to imagine, it is not at all simple to realize this condition in practice. In other words, if one were to determine this force by a simulation, the result must be independent of the system size. Too often in simulation studies this invariance property is not demonstrated, thus rendering the resulting defect driving force suspicious.

It is intuitive to expect that the invariance of the driving force is intimately connected to the question of how local are the interactions between the defect and its immediate surrounding in the system. If the effects are sufficiently local on the scale of separation distances between defects, then it is likely that a finite simulation cell with one or more defects is adequate to give the desired defect driving force. In any event it is clear that to establish invariance or study locality, one can perform simulation on cells of increasing size. Then the question is, what quantity should one calculate?

We propose to take a thermodynamic approach to this issue and consider a free-energy formulation [21]. We imagine separating our system into a core region (C) of interest with a buffer layer (L) between it and the remainder of the system (A). The interaction energy for the system then can be written as,

$$U_{\rm tot}(\mathbf{q}^N) = U(\mathbf{q}^{\rm A}) + U(\mathbf{q}^{\rm A}, \mathbf{q}^{\rm L}) + U(\mathbf{q}^{\rm L}, \mathbf{q}^{\rm C}) + U(\mathbf{q}^{\rm C}), \tag{9}$$

where an argument denotes the degrees of freedom in that particular region. Notice that regions C and A are coupled to the buffer region through the second and third terms respectively. With this decomposition one can evaluate the partition function by holding L fixed and integrating over C and A so that the Helmholtz free-energy becomes,

$$F_{\rm tot} = F_C(\mathbf{q}^L) + F_A(\mathbf{q}^L), \tag{10}$$

Now we consider a defect moving from one potential valley to the next (cf. Fig. 7) so that the energy change between initial and final configurations can be expressed as,

$$\Delta G_C \equiv \Delta F_{\rm tot} = \Delta F_C(\mathbf{q}^L) - \sum_{i\in L} \langle \mathbf{f}_i^{\rm ext} \rangle \cdot \Delta \langle \mathbf{q}_i^{\rm L} \rangle, \tag{11}$$

where $\langle\rangle$ denotes ensemble average, and G_C is the local (atomistic) Gibbs free energy which depends explicitly only on local knowledges of $\mathbf{q}^{\rm C}$ and $\mathbf{q}^L$, not $\mathbf{q}^A$. In writing Eq.(11) we have approximated the change in F_A to first order in the displacement $\mathbf{q}^L$; $\mathbf{f}_i^{\rm ext}$ being the force acting on L due to A.

Now we want to show that ΔG_C can play the role of an invariant with a specific example [21]. Consider a dumbbell self-interstitial in a bcc lattice of Fe atoms placed just 14Åaway from a surface, as shown in Fig. 9. The free surface provides a driving force for the interstitial to move toward the surface. The exact energy change for the interstitial to move one lattice constant, a repeat distance of 2.85Å, is calculated by performing full relaxations for the entire system before and after the move. The result is quite small, -0.00013921 eV. In Table 3 we show the results obtained by using Eq.(11) with various sizes for region C

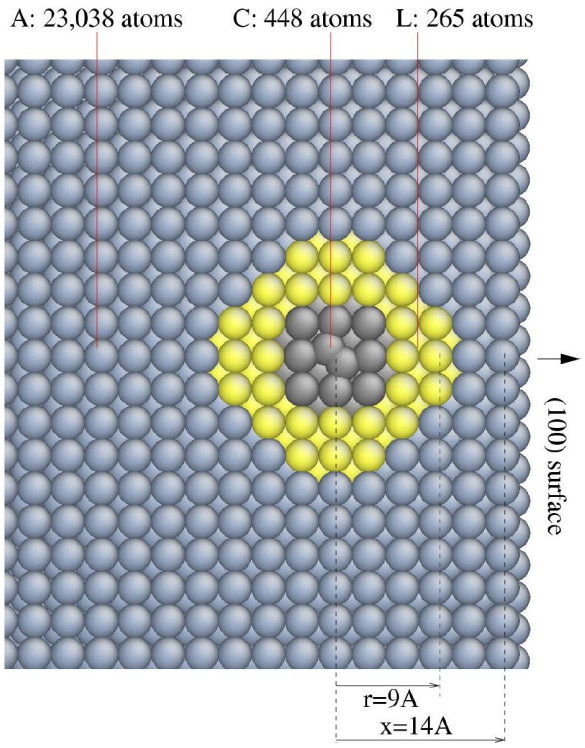

Figure 9: Migration of a ⟨110⟩ dumbbell self-interstitial in α-Fe near a (100) surface. [21]

and corresponding radius of the buffer region L. One can see that the convergence is quite satisfactory for a core size of 506 atoms. We have also obtained results for the energy change for a crack tip in the vicinity of a spherical hole, and a screw dislocation in the vicinity of another dislocation or a notch [21]. In all theses cases of a defect in the presence another defect, the exact energy change can be obtained to high accuracy using Eq.(11), with convergence achieved with region C containing no more than several hundred atoms. The implication is that the free-energy change formulated above is an appropriate measure of local defect driving force; it has the desired invariant property and is more robust and easier to use in practice than the conventional (local) stress approach for studying defect mobility by atomistic calculations.

7. Outlook

It is perhaps worthwhile to point out again that the importance of materials technology in our society combined with the advent of high performance computing has given rise to the current focus on multiscale materials modeling as a new component of computational materials research. This in turn provides exciting opportunities for the investigation of longstanding seemingly simple but fundamentally enduring issues where

r [Å]	C atoms	[eV]
8	170	-0.00022667
9	265	-0.00012683
10	338	-0.00013634
11	506	-0.00014005
12	610	-0.00013860
13	776	-0.00013856
14	952	-0.00013859
15	1240	-0.00013866

Table 3: Convergence of approximate free-energy change calculation for migration of a ⟨110⟩ dumbbell self-interstitial near a (100) surface in α-Fe [21]. Exact value is -0.00013921 eV.

atomistic inputs can lead to significant new insights. In this Commentary we have discussed illustrative results on strength and deformation which clearly bring out the important role of defect microstructure at the atomistic level. Three more examples may be briefly cited to emphasize that this type of development will be of growing interest.

For the predictive simulation of crystal plasticity a key question is how can quantitative knowledge of the dislocation core and atomistic methods for analyzing dislocation interactions be used to develop a mechanism-based description of strain hardening? In a large-scale molecular dynamics simulation of crack propagation, it was observed that a Lomer-Cottrell lock, formed by two intersecting Shockley partials, can be destroyed by the action of another partial nearby [65]. The critical stress for unzipping (destroying) the junction was estimated to be about 15 MPa, which is consistent with values previously deduced from experimental data, thus demonstrating the feasibility of linking molecular dynamics and dislocation dynamics simulations and eliminating the need for intermediate experimental input.

Atomistic simulation can play a similar role in our understanding of brittle-ductile behavior in fracture. The current continuum approach is to introduce an interplanar potential, equivalent to specifying a stress-displacement constitutive relation on the slip plane, associated with rigid block sliding in a homogeneous lattice. Through this potential one may introduce certain atomic-scale effects and therefore make the approach a continuum-atomistic hybrid. This strategy has been implemented, in part, in a molecular dynamics simulation in which dislocation emission from a crack tip under an applied tensile stress has been isolated and analyzed to produce the stress-displacement relation on activated slip plane before and after nucleation [66]. The results revealed clearly the essential

role of surface steps in the nucleation event and the effects of crack-tip shielding once the dislocation is emitted.

Another emerging and significant challenge for atomistic simulations is plastic flow in polycrystalline solids where the understanding of how crystal grains deform on decreasing length scales is needed [67]. It has been found recently from simulations of deforming nanocrystals that the well-known Hall-Petch effect where strength increases with decreasing grain size (in the micrometer range) does not hold in nanocrystals where the grain size is only a few nanometers; instead, a reverse Hall-Petch behavior was observed which could be attributed to small-scale sliding in the grain boundaries. This suggests the existence of a critical size separating the two types of behavior, which in turn implies that as grain size is reduced across this critical value, the deformation mechanism changes from the intragranular processes of dislocation nucleation and pile-up to intergranular sliding. A similar transition may occur in nanometer-scale electronic components, such as epitaxial films and quantum dots. In these heterostructures, the lattice mismatch between different materials induces strain, and how it relaxes during fabrication will determine the material structure, and hence its properties. Again, one expects competition between processes mediated by misfit defects such as dislocations, and surfaced-based processes such as roughening or morphological changes.

We conclude by returning to the opening theme of our discussion and noting from the Summary of the Report on National workshop on Advanced Scientific Computing, July 1998 [1], that success in any grand challenge enterprise will require not only science and technology, but also integration and partnership among its participants. We believe the field of materials science will be continually enriched as it expands to include scientists and engineers from a multidisciplinary range of background and interest, from physics and engineering, to chemistry, and to biology.

Acknowledgment - This work was supported by AFOSR (F49620-00-10082), NSF (DMR-9980015), Lawrence Livermore National Laboratory (ASCI-Level 2 grant), and Honda R&D, Ltd. We acknowledge longstanding collaborations with V. Bulatov, D. Wolf, A. S. Argon, J. F. Justo, M. Tang, J. Wang, F. Cleri and S. Phillpot.

REFERENCES

1. Report of the National Workshop on Advanced Scientific Computing, July 30-31, 1998 (National Academy of Sciences). Copies of the report may be obtained from website: http://www.er.doe.gov/production/octr/mics/.
2. Special Issue of J. Computer-Aided Mater. Design, vol. 3, (1996); special issue of Current Opinion in Solid State and Mater. Sci., vol. 3, no. 6 (1998).
3. G. H. Campbell, S. M. Foiles, H. Huang, D. A. Hughes, W. E. King, D. H. Lassila, D. J. Nikkel, T. D. de la Rubia, J. Y. Shu, V. P. Smyshlyaev, Mater. Sci. Eng., A251 (1998) 1.
4. M. Born, Proc. Cambridge Philos. Soc., 36 (1940) 160.
5. M. Born and K. Huang, Dynamical Theory of Crystal Lattices, Clarendon, Oxford (1956).
6. R. Hill, Mathematical Proceedings of the Cambridge Philosophical Society, 77 (1975) 225.
7. R. Hill and F. Milstein, Phys. Rev. B, 15 (1977) 3087.
8. A. Kelly and N. H. Macmillan, Strong Solids, 3rd ed., Clarendon, Oxford (1986).
9. J. Wang, J. Li, S. Yip, S. Phillpot, D. Wolf, Phys. Rev. B, 52 (1995) 12627.
10. D. C. Wallace, Thermodynamics of Crystals, Wiley, New York (1972).
11. Z. Zhou and B. Joos, Phys. Rev. B, 54 (1996) 3841.
12. J. W. Morris and C. R. Krenn, Philos Mag. A, 80 (2000) 2827.
13. T. H. K. Barron and M. L. Klein, Proc. Phys. Soc., 85 (1965) 523.
14. W. G. Hoover, A. C. Holt and D. R. Squire, Physica A, 44 (1969) 437.
15. Z. S. Basinski, M. S. Duesbery, A. P. Pogany, R. Taylor, Y. P. Varshni, Canadian Journal of Physics, 48 (1970) 1480.
16. J. Wang, S. Yip, S. Phillpot, D. Wolf, Phys. Rev. Lett., 71 (1993) 4182.
17. K. Mizushima, S. Yip, E. Kaxiras, Phys. Rev. B, 50 (1994) 14952.
18. M. Tang and S. Yip, J. Appl. Phys., 76 (1994) 2719.
19. F. Cleri, J. Wang and S. Yip, J. Appl. Phys., 77 (1995) 1449.
20. M. Tang and S. Yip, Phys. Rev. Lett., 75 (1995) 2738-41.
21. J. Li, Ph.D. Thesis, Massachusetts Institute of Technology (2000).
22. M. Born, J. Chem. Phys., 7 (1939) 591.
23. L. Hunter and S. Siegel, Phys. Rev., 61 (1942) 84.
24. S. M. Foiles, M. I. Baskes, M. S. Daw, Phys. Rev. B, 33 (1986) 7983.
25. M. Parrinello and A. Rahman, J. Appl. Phys., 52 (1981) 7182.
26. J. R. Ray, Comput. Phys. Rept., 8 (1988) 109.
27. J. Wang, J. Li, S. Yip, D. Wolf and S. Phillpot, Physica A, 240 (1997) 396.
28. L. L. Boyer, Phase Transitions, 5 (1985) 1.
29. J. F. Lutsko, D. Wolf, S. R. Phillpot, S. Yip, Phys. Rev. B, 40 (1989) 2841.
30. D. Wolf, P. R. Okamoto, S. Yip, J. F. Lutsko, M. Kluge, J. Mater. Res., 5 (1990) 286.
31. J. L. Tallon, Nature, 342 (1989) 658.
32. J. Tersoff, Phys. Rev. B, 39 (1989) 5566.

33. M. Tang, Ph.D. Thesis, Massachusetts Institute of Technology (1995).
34. H. Inui, H. Mori, A. Suzuki, H. Fujita, Philos. Mag. B, 65 (1992) 1.
35. M. Yoshida, A. Onodera, M. Ueno, K. Takemura, O. Shimomura, Phys. Rev. B, 48 (1993) 10587.
36. G. C. Serghiou, R. R. Winters, W. S. Hammack, Phys. Rev. Lett., 68 (1992) 331.
37. R. G. Greene, H. Luo, A. L. Ruoff, Phys. Rev. Lett., 73 (1994) 2476.
38. M. Hemmati, A. Chizmeshya, G. H. Wolf, P. H. Poole, J. Shao, C. A. Angell, Phys. Rev. B, 51 (1995) 14841.
39. J. S. Tse and D. D. Klug, Phys. Rev. Lett., 67 (1991) 3559.
40. N. Binggeli, N. R. Keskar, J. R. Chelikowsky, Phys. Rev. B, 49 (1994) 3075.
41. G. W. Watson and S. C. Parker, Phys. Rev. B, 52 (1995) 13306.
42. M. S. Duesbery and G. Y. Richardson, Crit. Rev. Solid State Mater. Sci., 17 (1991) 1.
43. J. P. Hirth and J. Lothe, Theory of Dislocations, Wiley, New York, (1982), p. 373.
44. H. J. Moller, Acta Metall., 26 (1978) 963.
45. R. W. Nunes, J. Bennetto, D. Vanderbilt, Phys. Rev. Lett., 77 (1996) 1516.
46. V. V. Bulatov, J. F. Justo, W. Cai, S. Yip, Phys. Rev. Lett., 79 (1997) 5042.
47. R. W. Nunes, J. Bennetto, D. Vanderbilt, Phys. Rev. B, 57 (1998) 10388.
48. V. V. Bulatov, S. Yip, A. S. Argon, Philos. Mag. A, 72 (1995) 453.
49. J. F. Justo, M. Z. Bazant, E. Kaxiras, V. V. Bulatov, S. Yip, Phys. Rev. B, 58 (1998) 2539.
50. S. Oberg, P. K. Stitch, R. Jones, M. I. Heggie, Phys. Rev. B, 51 (1995) 13138.
51. A. Valladares, J. A. White and A. P. Sutton, Phys. Rev. Lett., 81 (1998) 4903.
52. W. Cai, V. V. Bulatov, J. F. Justo, A. S. Argon, S. Yip, Phys. Rev. Lett., 84 (2000) 3346.
53. W. Cai, V. V. Bulatov, S. Yip, J. Computer-Aided Materials Design, 6 (1999) 175.
54. H. Alexander, in Dislocation in Solids, F. R. N. Nabarro, ed., North-Holland, Amsterdam, (1986) vol. 7, p. 113.
55. W. Benoit, M. Bujard, G. Gremaud, Phys. Status Solidi A, 104 (1987) 427.
56. G. Schoeck, Scr. Metall. Mater., 30 (1994) 611.
57. F. R. N. Nabarro, Philos. Mag. A, 75 (1997) 703.
58. V. Celli, M. Kabler, T. Ninomiya, R. Thomson, Phys. Rev., 131 (1963) 58.
59. Y. Fujii, N. A. Lurie, R. Pynn, G. Shirane, Phys. Rev. B, 10 (1974) 3647.
60. J. F. Justo, V. V. Bulatov, and S. Yip, J. Appl. Phys., 86 (1999) 4249.
61. Y. M. Huang, J. C. H. Spence and O. F. Sankey, Phys. Rev. Lett., 74 (1995) 3392.
62. P. B. Hirsch, A. Ourmazd and P. Pirouz, Inst. Phys. Conf. Ser., 60 (1981) 29.
63. H. Gottschalk, H. Alexander and V. Dietz, Inst. Phys. Conf. Ser., 87 (1987) 339.
64. H. R. Kolar, J. C. H. Spence and H. Alexander, Phys. Rev. Lett., 77 (1996) 4031.
65. V. Bulatov, F. Abraham, L. Kubin, B. Devincre, S. Yip, Nature, 391 (1998) 669.
66. F. Cleri, S. Yip, D. Wolf, S. R. Phillpot, Phys. Rev. Lett., 79 (1997) 1309.
67. S. Yip, Nature, 391 (1998) 532.